

MAX 4 and MAX 5 CMB anisotropy measurement constraints on open and flat- Λ CDM cosmogonies

Ken Ganga¹, Bharat Ratra², Mark A. Lim³, Naoshi Sugiyama⁴, and Stacy T. Tanaka⁵

Received _____; accepted _____

arXiv:astro-ph/9708202v1 22 Aug 1997

¹IPAC, MS 100-22, California Institute of Technology, Pasadena, CA 91125.

²Department of Physics, Kansas State University, Manhattan, KS 66506.

³Department of Physics, University of California, Santa Barbara, CA 93106.

⁴Department of Physics, Kyoto University, Kitashirakawa-Oiwakecho, Sakyo-ku, Kyoto 606.

⁵Department of Physics, University of California, Berkeley, CA 94720.

ABSTRACT

We account for experimental and observational uncertainties in likelihood analyses of cosmic microwave background (CMB) anisotropy data from the MAX 4 and MAX 5 experiments. These analyses use CMB anisotropy spectra predicted in open and spatially-flat Λ cold dark matter cosmogonies. Amongst the models considered, the combined MAX data set is most consistent with the CMB anisotropy shape in $\Omega_0 \sim 0.1 - 0.2$ open models and less so with that in old ($t_0 \gtrsim 15 - 16$ Gyr, i.e., low h), high baryon density ($\Omega_B \gtrsim 0.0175h^{-2}$), low density ($\Omega_0 \sim 0.2 - 0.4$), flat- Λ models. The MAX data alone do not rule out any of the models we consider at the 2σ level.

Model normalizations deduced from the combined MAX data are consistent with those drawn from the UCSB South Pole 1994 data, except for the flat bandpower model where MAX favours a higher normalization. The combined MAX data normalization for open models with $\Omega_0 \sim 0.1 - 0.2$ is higher than the upper 2σ value of the DMR normalization. The combined MAX data normalization for old (low h), high baryon density, low-density flat- Λ models is below the lower 2σ value of the DMR normalization. Open models with $\Omega_0 \sim 0.4 - 0.5$ are not far from the shape most favoured by the MAX data, and for these models the MAX and DMR normalizations overlap. The MAX and DMR normalizations also overlap for $\Omega_0 = 1$ and some higher h , lower Ω_B , low-density flat- Λ models.

Subject headings: cosmic microwave background — cosmology: observations — large-scale structure of the universe

1. Introduction

Recent measurements of spatial anisotropy in the cosmic microwave background indicate that CMB anisotropy data will soon provide useful constraints on cosmological parameters such as Ω_0 , h , and Ω_B (Bennett et al. 1996; Ganga et al. 1994; Gutiérrez et al. 1997; Piccirillo et al. 1997; Netterfield et al. 1997; Gundersen et al. 1995; Tucker et al. 1997; Platt et al. 1997; Masi et al. 1996; Lim et al. 1996, hereafter L96; Cheng et al. 1997; Griffin et al. 1997; Scott et al. 1996; Leitch et al. 1997; Church et al. 1997, see Page 1997 for a review). Here, the present value of the (total) nonrelativistic-mass density parameter Ω_0 , is $8\pi G\rho_b(t_0)/(3H_0^2)$, where G is the gravitational constant, $\rho_b(t_0)$ is the mean nonrelativistic-mass density now, $H_0 = 100h$ km s⁻¹ Mpc⁻¹ is the Hubble parameter now, and Ω_B is the current value of the baryonic-mass density parameter.

Ganga et al. (1997a, hereafter GRGS) developed general methods to account for experimental and observational uncertainties, such as beamwidth and calibration uncertainties, in likelihood analysis of CMB data sets. These methods have previously been used in conjunction with theoretically-predicted CMB anisotropy spectra in analyses of the Gundersen et al. (1995) SP94 data and the Church et al. (1997) SuZIE data (GRGS; Ganga et al. 1997b). Bond & Jaffe (1997) have also analyzed the SP94 data and the Netterfield et al. (1997) SK data.

In this paper we present results from a similar analysis of the MAX 4 and MAX 5 CMB anisotropy data sets (Devlin et al. 1994; Clapp et al. 1994; Tanaka et al. 1996, hereafter T96; L96). MAX 4 and MAX 5 are the most recent of the published balloon-borne MAX CMB anisotropy experiments. The original MAX detector and the MAX 1 results are discussed in Fischer et al. (1992). The ACME telescope used in these MAX experiments is described in Meinhold et al. (1993a). The MAX 2 observational results are in Alsop et al. (1992). Meinhold et al. (1993b) and Gundersen et al. (1993) present the MAX 3 results. Analyses of the MAX 3 observations, in the context of the fiducial CDM model, is given in Srednicki et al. (1993) and Dodelson & Stebbins (1994).

Descriptions of MAX 4 and 5 are given in Devlin et al. (1994), Clapp et al. (1994), T96, and L96; we review here the information needed for our analyses. Data were taken in four frequency bands centered at 3.5, 6, 9, and 14 cm^{-1} ; our analyses do not use the 14 cm^{-1} band data. The FWHM of the beams, assumed to be gaussian, are: $0.55^\circ \pm 0.05^\circ$ for the MAX 4 3.5 cm^{-1} band, $0.75^\circ \pm 0.05^\circ$ for the MAX 4 6/9 cm^{-1} bands, $0.5(1 \pm 0.10)^\circ$ for the MAX 5 3.5 cm^{-1} band, and $0.55(1 \pm 0.10)^\circ$ for the MAX 5 6/9 cm^{-1} bands, where the uncertainties are one standard deviation. The MAX data used here were taken during smooth, constant velocity, constant declination, azimuthal scans extending 6° on the sky for MAX 4 and 8° on the sky for MAX 5. While observing, the beam was sinusoidally chopped with a half peak-to-peak amplitude of 1.4° on the sky. The data were coadded into 21 bins for MAX 4 and 29 bins for MAX 5.

MAX 4 data were taken in smooth scans of $\pm 3^\circ$ on the sky centered near the stars γ Ursae Minoris, ι Draconis (hereafter 4ID), and σ Herculis (hereafter 4SH). Sky rotation has a significant effect on the γ Ursae Minoris scan pattern (Devlin et al. 1994), so we do not analyze this data set here. The bin positions in the released 4ID and 4SH data sets are data-weighted averages (A. Clapp, private communication 1996); we use evenly spaced bins in this analysis. MAX 5 data were taken in smooth scans of $\pm 4^\circ$ on the sky centered near the stars HR5127 (hereafter 5HR), μ Pegasi (hereafter 5MP), and ϕ Herculis (hereafter 5PH). The 9 cm^{-1} 5PH data is thought to contain atmospheric emission (T96, 5PH data was taken at lower balloon altitude), and is not used for CMB anisotropy analyses. The 5MP data has structure that correlates with *IRAS* 100 μm dust emission (L96). Off-diagonal noise correlations affect the 5HR and 5PH results by $\lesssim 2\%$ (T96), and are ignored here.

MAX 4 and 5 were calibrated primarily by using a membrane transfer standard (Fischer et al. 1992); the absolute calibration uncertainty is 10% (1σ).

In §2 we summarize some of the computational techniques used in our analysis. Our results and a discussion are in §3, and we conclude in §4.

2. Summary of Computation

Our conventions, notation, and techniques are those of GRGS.

The CMB anisotropy spectra for some of the models we consider here are shown in Figure 1. The models are described in Ratra et al. (1997) and GRGS, and the computation of the spectra is discussed in Sugiyama (1995). Besides the flat bandpower and fiducial CDM models, we also consider open and flat- Λ CDM cosmogonies. The models assume gaussian, adiabatic, primordial energy-density power spectra. The flat- Λ models assume a scale-invariant energy-density power spectrum (Harrison 1970; Peebles & Yu 1970; Zel’dovich 1972), as is found in the simplest spatially-flat inflation models (Guth 1981, also see Kazanas 1980; Sato 1981a,b). The open models assume the energy-density power spectrum (Ratra & Peebles 1994, 1995; Bucher, Goldhaber, & Turok 1995; Yamamoto, Sasaki, & Tanaka 1995) of the simplest open-bubble inflation models (Gott 1982; Guth & Weinberg 1983). The model spectra are parameterized by the quadrupole-moment amplitude of the CMB anisotropy, $Q_{\text{rms-PS}}$, as well as Ω_0 , h , and Ω_B . The spectra shown in Figure 1 are normalized to the DMR maps (Górski et al. 1996,1998; Stompor 1997). Parameter values for the models considered are given in Table 6.

The low-density models considered here are the simplest ones roughly consistent with most current observations. For flat- Λ models see Kitayama & Suto (1996), Ratra et al. (1997), Bunn & White (1997), Turner (1997), Peacock (1997), and Cole et al. (1997), and for the open case see Kitayama & Suto (1996), Ratra et al. (1997), Górski et al (1998), Gott (1997), Peacock (1997), and Cole et al. (1997). The values of the parameters Ω_0 , h , and Ω_B used here are chosen to be roughly consistent with present observational estimates of Ω_0 , h , the age of the universe, and the constraints on Ω_B that follow from standard nucleosynthesis (Ratra et al. 1997). In this analysis we ignore the effects of tilt, primordial gravity waves, and reionization. These effects are unlikely to be significant in viable open models.⁶ In order to reconcile some of the flat- Λ models with

⁶ Maia & Lima (1996), Tanaka & Sasaki (1997), and Bucher & Cohn (1997) have studied primordial gravity waves in the open model. Initial indications are that predictions based on

observational data, however, some such effect is needed to suppress intermediate-scale (CMB and matter) and small-scale (matter) power (Stompor, Górski, & Banday 1995; Ostriker & Steinhardt 1995; Ratra et al. 1997; Klypin, Primack, & Holtzman 1996; Ganga, Ratra, & Sugiyama 1996; Maddox, Efstathiou, & Sutherland 1996; Peacock 1997; Cole et al. 1997).

Figure 1 also shows the four different zero-lag window functions, W_l , for the individual MAX channels at their nominal beamwidths. The usual window function parameters, the value of l where W_l is largest, l_m , the two values of l where $W_{l_{e-0.5}} = e^{-0.5}W_{l_m}$, $l_{e-0.5}$, and the effective multipole, l_e , are given in Table 1 for these window functions (e.g., Bond 1996; GRGS).

Figure 2 shows the moments $(\delta T_{\text{rms}}^2)_l$ for two MAX window functions and some selected CMB anisotropy spectra (GRGS, eqs. [5] & [6]). Given an assumed CMB anisotropy spectrum, these moments provide a convenient measure of the range of l to which MAX is sensitive. Table 2 gives l_m , the value of l at which $(\delta T_{\text{rms}}^2)_l$ is largest, and $l_{e-0.5}$ the two multipoles where $(\delta T_{\text{rms}}^2)_{l_{e-0.5}} = e^{-0.5}(\delta T_{\text{rms}}^2)_{l_m}$, for the MAX window functions and the models we consider. As is true for SP94 and SuZIE, the range of multipole moments to which each window function is sensitive is quite model dependent (GRGS; Ganga et al. 1997b).

The reduced MAX 4 and MAX 5 data are shown in Figure 3. In Table 3, the column labelled “Sky” indicates the estimated anisotropy rms for those individual channel data sets thought to be purely CMB anisotropy. This is computed from the data of Figure 3 as the square root of the difference between the variance of the mean temperatures and the variance of the error bars.

The computation of the likelihood function is described in GRGS. The only difference between what is done here and in GRGS is that for the 5MP data (but not the other data sets) we also marginalized over a possible dust contamination given by the spectrum in L96 and an arbitrary spatial morphology. Beamwidth and calibration uncertainties are accounted for as described in GRGS. We again use three-point Gauss-Hermite quadrature to marginalize over beamwidth

the simplest observationally-viable single-scalar-field open-bubble-inflation energy-density power spectrum (Ratra & Peebles 1994, 1995) are negligibly affected by primordial gravity waves.

uncertainty.

In Table 3, the column labelled “FBP” lists central δT_{rms} values derived from likelihood analyses using the flat bandpower (FBP) spectrum.

To derive the $Q_{\text{rms-PS}}$ central value and limits from the likelihood function we assume a uniform prior in $Q_{\text{rms-PS}}(\geq 0)$. The central value is taken to be the value of $Q_{\text{rms-PS}}$ at which the probability density distribution peaks. The MAX limits we quote are $\pm 1\sigma$ highest posterior density (HPD) limits for (2σ HPD) detections. For nondetections we quote upper 2σ equal tail (ET) limits.⁷

In Table 4 we give bandtemperature ($\delta T_l = \delta T_{\text{rms}} / [\sum_{l=2}^{\infty} [(l + 0.5)W_l / \{l(l + 1)\}]^{0.5}$, e.g., Bond 1996; GRGS, eq. [7]) central values and $\pm 1\sigma$ limits derived from flat bandpower likelihood analyses of the individual-channel MAX data sets. The last two columns give the average of the $\pm 1\sigma$ error bars in μK and as a percentage of the central value. In Table 5 we give the corresponding numerical values derived from flat bandpower likelihood analyses of the combined-channel MAX data sets.

Central values and limits for $Q_{\text{rms-PS}}$ are given in Tables 6 and 7 for the various individual and combined MAX data sets. Some of the likelihood functions used to derive these numerical values are shown in Figure 4. Tables 6 and 7 also show the results from analyses of the DMR data, accounting for both statistical and systematic DMR uncertainties (Górski et al. 1996,1998; Stompor 1997). The DMR limits quoted are $\pm 2\sigma$ HPD for the two extreme data sets: (1) galactic-frame maps accounting for the high-latitude Galactic emission correction and including the $l = 2$ moment in the analysis; and (2) ecliptic-frame maps ignoring the high-latitude Galactic

⁷ ET limits are determined by integrating the probability density distribution function starting from 0 μK . The 2σ ET limit encompasses 97.7% of the area. HPD limits are determined by integrating the probability density distribution function starting at the peak and minimizing the difference between the upper and lower limits. The 1σ and 2σ HPD limits encompass 68.3% and 95.5% of the area, respectively. See GRGS for a discussion.

correction and excluding the $l = 2$ moment. The DMR central values quoted are the arithmetic mean of the $\pm 2\sigma$ limits. See Górski et al. (1998) for a discussion of the DMR central values and limits.

Tables 8 and 9 give the values of the probability density distribution functions at the peak, and the marginalized (over $Q_{\text{rms-PS}}$) probability density distribution values for the various combined-channel MAX data sets.⁸ The models shown in the figures were chosen on the basis of their marginal probability distribution values for the C(ombined) MAX data set. Model O1 (an $\Omega_0 = 0.1$, open model) is the most likely model, followed, among the selected models, by Flat (flat bandpower), O14 (fiducial CDM), models $\Lambda 2$ and O11 (a spatially-flat, $\Omega_0 = 0.2$ model and an open, $\Omega_0 = 0.5$ model), and the least likely one, $\Lambda 10$ (a flat- Λ , $\Omega_0 = 0.4$ model). These selected models include the most and least likely open and flat- Λ ones among those considered.

3. Results and Discussion

From Table 3 we see that, for those channels with 2σ HPD detections, the rms estimated from likelihood analyses using flat bandpower spectra is in good agreement with the “sky” rms estimated from the data, especially for MAX 5. The exception is 4ID 6 cm^{-1} ; based on the SP94 analyses (GRGS), it is unlikely that this can significantly affect conclusions drawn from the combined MAX data sets.

Tables 4 and 5 give the central values and $\pm 1\sigma$ limits on bandtemperature derived from likelihood analyses with the flat bandpower spectrum. These numerical values can not be compared directly to those of T96 and L96 because of the many differences in the analyses. For instance, beamwidth and calibration uncertainties are accounted for in different ways, and T96 use a likelihood ratio method while we use a maximum likelihood method (see T96 for discussion). Nevertheless, it is reassuring that the largest differences are not greater than $\sim 1\sigma$.

⁸ These values are computed using a uniform prior in $Q_{\text{rms-PS}}$. The following conclusions are therefore based solely on the MAX data.

From Tables 4 and 5, we note that the deduced 4SH average absolute uncertainty is larger than that of the 4SH 9 cm⁻¹ channel and only slightly smaller than the 4SH 3.5 cm⁻¹ one. Similarly, the deduced 5PH average absolute uncertainty is only slightly smaller than the 5PH 3.5 and 6 cm⁻¹ ones. On the other hand, the average absolute uncertainties do shrink when the 4ID or 5HR individual-channel data sets are combined.

These error bars only account for instrumental and atmospheric noise, sample variance due to the limited number of independent data pixels, and beamwidth and calibration uncertainty. For purely CMB anisotropy data, instrumental and atmospheric noise should integrate down with more channels of data, sample variance should not, and the beamwidth and calibration uncertainties are negligible for the purposes of this discussion. Since the MAX 4 3.5 and 6/9 cm⁻¹ window functions are rather dissimilar, an analysis of the behaviour of the error bars in this case will require a numerical simulation. We focus here on the 5HR and 5PH data sets.

We follow the analysis of §3 of GRGS. In their notation, the total average absolute δT_l error bars for the combined-channel ($\sigma_{\text{tot.,com.}}$) and individual-channel ($\sigma_{\text{tot.,ind.}}$) data sets are, from Tables 4 and 5,

$$\begin{aligned} \sigma_{\text{tot.,ind.}}^{5\text{HR}} &= 13 \mu\text{K}, & \sigma_{\text{tot.,com.}}^{5\text{HR}} &= 8.4 \mu\text{K}, \\ \sigma_{\text{tot.,ind.}}^{5\text{PH}} &= 22 \mu\text{K}, & \sigma_{\text{tot.,com.}}^{5\text{PH}} &= 21 \mu\text{K}. \end{aligned} \tag{1}$$

To get this behaviour, the sample variance (σ_{SV}) and intrinsic noise (σ_{N}) contributions to the δT_l error bars need to be

$$\begin{aligned} \sigma_{\text{SV}}^{5\text{HR}} &= 5.0 \mu\text{K}, & \sigma_{\text{N}}^{5\text{HR}} &= 12 \mu\text{K}, \\ \sigma_{\text{SV}}^{5\text{PH}} &= 20 \mu\text{K}, & \sigma_{\text{N}}^{5\text{PH}} &= 9.3 \mu\text{K}; \end{aligned} \tag{2}$$

i.e., the 5HR data needs to be dominated by intrinsic noise while the 5PH data needs to be dominated by sample variance. To see if this is reasonable, we now estimate the MAX 5 sample variance, following the discussion of GRGS based on the simulations of Netterfield et al. (1995). We approximate the MAX 5 individual-channel beamwidths by $\sigma_{\text{FWHM}} = 0.5^\circ$; the 8° scans then have 16 independent pixels (with 29 bins, MAX 5 is quite oversampled). With the Netterfield et

al. (1995) 10% simulation correction to the analytic estimate of sample variance (GRGS), the MAX 5 sample variance is 19% of the δT_l central value. Using this, the 5HR and 5PH δT_l central values of Table 5, and the standard equations, we find for the sample variance and intrinsic noise contributions to the 5HR and 5PH δT_l average error bars,

$$\begin{aligned} \sigma_{\text{SV}}^{5\text{HR}} &= 5.3 \mu\text{K}, & \sigma_{\text{N}}^{5\text{HR}} &= 12 \mu\text{K}, \\ \sigma_{\text{SV}}^{5\text{PH}} &= 14 \mu\text{K}, & \sigma_{\text{N}}^{5\text{PH}} &= 17 \mu\text{K}. \end{aligned} \tag{3}$$

This approximate estimate of the 5HR sample variance and intrinsic noise is very close to what is needed (eq. [2]) to explain the behaviour of the 5HR error bars. However, eq. (3) indicates that the 5PH sample variance is not as large as needed (eq. [2]) to explain the behaviour of the 5PH error bars. While it is premature to read much from such an approximate analysis (GRGS), we note that the 5PH data were taken at lower balloon altitude and that the 5PH 9 cm^{-1} data can not be used for analyses of CMB anisotropy (T96).

We do not record here δT_l numerical values for other models from the individual-channel MAX data sets (the flat bandpower model values are in Table 4). As was the case for SP94 (GRGS), for a given MAX data set the deduced δT_l values vary by $\sim 0\text{-}10\%$ from model to model, with a typical range of $\sim 5\%$. This is significantly smaller than the variations for SuZIE (Ganga et al. 1997b).

The 5MP data do not show a 2σ HPD detection. Because of the significant non-CMB component in this data set (L96), and the need for “subtraction” prior to CMB anisotropy analysis (L96), there is the worry that this data set might be biased. Fortunately, as is seen from the 5, 5noMP, C(ombined), and CnoMP entries in Table 5, inclusion/exclusion of 5MP shifts the deduced normalization only by $\sim 0.8\sigma$, so 5MP does not significantly affect the final results. We note that the 5MP upper limit is quite consistent with the 4ID and 5HR detections, but is somewhat below the 4SH and 5PH detections. Given the discussion about sample variance and intrinsic noise uncertainties above, we believe that it is more reasonable to include the 5MP results.

Tables 6 – 9 summarize our MAX data set analyses.

Table 8 lists the maximum values of the probability density distribution function for the various combined-channel MAX data sets and all models considered here. From these numerical values, and from Figure 4, one sees that for all the combined-channel MAX data sets, except 5MP which does not have a detection, the likelihood functions are peaked and very well separated from $0 \mu\text{K}$. Note the 14% error bar for the C(ombined) data set in Table 5; the combined MAX data shows a very significant detection, even after calibration and beamwidth uncertainties are accounted for. For comparison, depending on model, the corresponding DMR error bars are $\sim 10 - 12\%$ (Górski et al. 1998). Given such likelihood functions, it is reasonable to choose between models on the basis of the value of the marginal probability distribution function.

Table 9 lists the marginal probability distribution values for the combined-channel MAX data sets. In all cases, among all the models considered here, the MAX data favour low-density open models with $\Omega_0 \sim 0.1 - 0.2$ (models O1 – O4).⁹ This is consistent with what we find from all the individual-channel MAX data sets (not shown here), and with what is found from an analysis of the SP94 data (GRGS). Our marginal probability distribution function is evaluated at isolated points in model-parameter $(\Omega_0, h, \Omega_B h^2)$ space; assuming it is a gaussian, a model 1σ away from the most favoured low-density open model CMB anisotropy shape has a marginal value of 0.61, and a model with marginal value 0.38 is 1.4σ away from the most favoured low-density open model. The C(ombined) MAX data set values of Table 9 do distinguish between models, although not at a very significant level.

We conclude that the MAX data are most consistent with the CMB anisotropy shape in

⁹ Figure 4a shows that the likelihood functions for all the combined-channel MAX data sets are significantly nongaussian. Consequently, conclusions about model viability based on the marginal probability density need not be identical to those drawn from the projected probability density. From Tables 8 and 9 one sees that the projected probability density does not distinguish as much between models as does the marginal probability distribution, and in fact weakly favours $\Omega_0 = 1$ over the open $\Omega_0 = 0.1$ case for the C(ombined) data.

low-density open CDM models with $\Omega_0 \sim 0.1 - 0.3$ and $0.4 - 0.5$ (with larger h and smaller Ω_B), and with the flat bandpower shape, among the models we consider here. The fiducial CDM and flat- Λ models have CMB anisotropy spectral shapes which MAX does not favour. This is especially true for old ($t_0 \gtrsim 15 - 16$ Gyr), large baryon density ($\Omega_B \gtrsim 0.0175h^{-2}$), low-density ($\Omega_0 \sim 0.2 - 0.4$), flat- Λ models. These results are consistent with those based on an analysis of the SP94 data (GRGS), as well as with earlier analyses of multiple CMB anisotropy data points (Ratra et al. 1997; Ganga et al. 1996; also see Hancock et al. 1997). We emphasize that, under the gaussian marginal assumption, the MAX data alone do not rule out any of the models we consider here at the 2σ level.

Tables 6 and 7 list the $Q_{\text{rms-PS}}$ values derived from the various combined-channel MAX data sets. These normalizations are in striking agreement with those deduced from the SP94 data (GRGS), except for the flat bandpower model where MAX favours a higher normalization than does SP94. This is further confirmation that the observed CMB anisotropy spectrum rises towards large l (Scott, Silk, & White 1995; Ratra et al. 1997; Ganga et al. 1996; Netterfield et al. 1997; Hancock et al. 1997; Page 1997; Lineweaver et al. 1997; Rocha & Hancock 1997).¹⁰

For open models with $\Omega_0 \sim 0.1 - 0.2$ the combined MAX data normalization is above the upper 2σ DMR normalization (Górski et al. 1998); for $\Omega_0 \sim 0.1$ it is also above the SuZIE 2σ upper limit (Ganga et al. 1997b). For the older (smaller h), higher Ω_B , flat- Λ models, the combined MAX normalization is below the lower 2σ DMR normalization (Stompor 1997). Both of these results are consistent with earlier CMB anisotropy conclusions (Ratra et al. 1997; Ganga et al. 1996). An open model with $\Omega_0 \sim 0.4 - 0.5$ and $h \sim 0.65$ has a CMB anisotropy spectral shape

¹⁰ The steepness of the rise towards large l depends on which data sets are included in the analysis. Hancock et al. (1997), Lineweaver et al. (1997), and Rocha & Hancock (1997) favour a slightly steeper C_l than do Ganga et al. (1996). This is because Ganga et al. (1996) include a number of data points (e.g., the four MSAM points and the MAX 3MP point which is consistent with the repeat 5MP result and the 4ID and 5HR measurements) which favour shallower C_l spectra.

which is not far from what is favoured by the MAX data; in addition, the MAX normalization for such a model is consistent with what is deduced from the DMR (Górski et al. 1998) and SP94 data (GRGS), and is also consistent with the SuZIE 2σ upper limit (Ganga et al. 1997b). The MAX and DMR normalizations also overlap for $\Omega_0 = 1$ and some higher h , lower Ω_B , low-density flat- Λ models.

4. Conclusion

We have accounted for beamwidth- and calibration-uncertainty in likelihood analyses of the MAX 4 and MAX 5 observational data that make use of theoretical CMB spatial anisotropy spectra in open and spatially-flat Λ CDM cosmogonies. In our analyses, we have assumed that the appropriately reduced MAX data is purely CMB spatial anisotropy. Other general caveats may be found in §4 of GRGS, and it is prudent to bear these in mind when interpreting our results.

The marginal probability distribution function values indicate that the MAX data favour low-density open models over older, high Ω_B , low-density, flat- Λ models. However, no model considered here is ruled out at the 2σ level by the MAX data alone, at least in the gaussian marginal probability distribution approximation. Combined with results from the analyses of the DMR, SP94, and SuZIE data, we find that $\Omega_0 \sim 0.1 - 0.2$ open models have CMB anisotropy spectra shallower than what is favoured by the observations while low h , high Ω_B flat- Λ models have spectra steeper than what is favoured by the observations, in agreement with earlier analyses.

It is interesting that the MAX and SP94 data sets lead to almost identical conclusions for observationally-motivated low-density open and flat- Λ CDM models. If confirmed, this result might be of some passing significance.

We acknowledge helpful discussions with A. Clapp, J. Cohn, J. Gundersen, S. Hanany, A. Lee, G. Rocha, and R. Stompor, as well as, especially, M. Devlin and L. Page. BR acknowledges support from NSF grant EPS-9550487 with matching support from the state of Kansas and from a

K*STAR First award. This work was partially carried out at the Infrared Processing and Analysis Center and the Jet Propulsion Laboratory of the California Institute of Technology, under a contract with the National Aeronautics and Space Administration.

REFERENCES

- Alsop, D. C., et al. 1992, *ApJ*, 395, 317
- Bennett, C. L., et al. 1996, *ApJ*, 464, L1
- Bond, J. R. 1996, in *Cosmology and Large Scale Structure*, ed. R. Schaeffer, J. Silk, M. Spiro, & J. Zinn-Justin (Amsterdam: Elsevier Science), 469
- Bond, J. R., & Jaffe, A. 1997, in *Microwave Background Anisotropies*, ed. F. R. Bouchet & T. T. Van (Gif sur Yvette: Editions Frontières), in press
- Bucher, M., & Cohn, J. D. 1997, *Phys. Rev. D*, 55, 7461
- Bucher, M., Goldhaber, A. S., & Turok, N. 1995, *Phys. Rev. D*, 52, 3314
- Bunn, E. F., & White, M. 1997, *ApJ*, 480, 6
- Cheng, E. S., et al. 1997, *ApJ*, submitted
- Church, S. E., et al. 1997, *ApJ*, 484, 523
- Clapp, A. C., et al. 1994, *ApJ*, 433, L57
- Cole, S., Weinberg, D. H., Frenk, C. S., & Ratra, B. 1997, *MNRAS*, 289, 37
- Devlin, M. J., et al. 1994, *ApJ*, 430, L1
- Dodelson, S., & Stebbins, A. 1994, *ApJ*, 433, 440
- Fischer, M. L., et al. 1992, *ApJ*, 388, 242
- Ganga, K., Page, L., Cheng, E., & Meyer, S. 1994, *ApJ*, 432, L15
- Ganga, K., Ratra, B., & Sugiyama, N. 1996, *ApJ*, 461, L61
- Ganga, K., Ratra, B., Gundersen, J. O., & Sugiyama, N. 1997a, *ApJ*, 484, 7 (GRGS)
- Ganga, K., et al. 1997b, *ApJ*, 484, 517
- Górski, K. M., et al. 1996, *ApJ*, 464, L11
- Górski, K. M., Ratra, B., Stompor, R., Sugiyama, N., & Banday, A. J. 1998, *ApJS*, 114, in press

- Gott III, J. R. 1982, *Nature*, 295, 304
- Gott III, J. R. 1997, in *Critical Dialogues in Cosmology*, ed. N. Turok (Singapore: World Scientific), in press
- Griffin, G. S., et al. 1997, in preparation
- Gundersen, J. O., et al. 1993, *ApJ*, 413, L1
- Gundersen, J. O., et al. 1995, *ApJ*, 443, L57
- Guth, A. 1981, *Phys. Rev. D*, 23, 347
- Guth, A. H., & Weinberg, E. J. 1983, *Nucl. Phys. B*, 212, 321
- Gutiérrez, C. M., et al. 1997, *ApJ*, 480, L83
- Hancock, S., Rocha, G., Lasenby, A. N., & Gutiérrez, C. M. 1997, *MNRAS*, in press
- Harrison, E. R. 1970, *Phys. Rev. D*, 1, 2726
- Kazanas, D. 1980, *ApJ*, 241, L59
- Kitayama, T., & Suto, Y. 1996, *ApJ*, 469, 480
- Klypin, A., Primack, J., & Holtzman, J. 1996, *ApJ*, 466, 13
- Leitch, E. M., Myers, S. T., Readhead, A. C. S., & Pearson, T. J. 1997, in preparation
- Lim, M. A., et al. 1996, *ApJ*, 469, L69 (L96)
- Lineweaver, C. H., Barbosa, D., Blanchard, A., & Bartlett, J. G. 1997, *A&A*, 322, 365
- Maddox, S. J., Efstathiou, G., & Sutherland, W. J. 1996, *MNRAS*, 283, 1227
- Maia, M. R. G., & Lima, J. A. S. 1996, *Phys. Rev. D*, 54, 6111
- Masi, S., et al. 1996, *ApJ*, 463, L47
- Meinhold, P. R., et al. 1993a, *ApJ*, 406, 12
- Meinhold, P. R., et al. 1993b, *ApJ*, 409, L1
- Netterfield, C. B., Jarosik, N., Page, L., Wilkinson, D., & Wollack, E. 1995, *ApJ*, 445, L69

- Netterfield, C. B., Devlin, M. J., Jarosik, N., Page, L., & Wollack, E. J. 1997, *ApJ*, 474, 47
- Ostriker, J. P., & Steinhardt, P. J. 1995, *Nature*, 377, 600
- Page, L. A. 1997, astro-ph/9703054
- Peacock, J. A. 1997, *MNRAS*, 284, 885
- Peebles, P. J. E., & Yu, J. T. 1970, *ApJ*, 162, 815
- Piccirillo, L., et al. 1997, *ApJ*, submitted
- Platt, S. R., Kovac, J., Dragovan, M., Peterson, J. B., & Ruhl, J. E. 1997, *ApJ*, 475, L1
- Ratra, B., & Peebles, P. J. E. 1994, *ApJ*, 432, L5
- Ratra, B., & Peebles, P. J. E. 1995, *Phys. Rev. D*, 52, 1837
- Ratra, B., Sugiyama, N., Banday, A. J., & Górski, K. M. 1997, *ApJ*, 481, 22
- Rocha, G., & Hancock, S. 1997, in *Microwave Background Anisotropies*, ed. F. R. Bouchet & T. T. Van (Gif sur Yvette: Editions Frontières), in press
- Sato, K. 1981a, *Phys. Lett. B*, 99, 66
- Sato, K. 1981b, *MNRAS*, 195, 467
- Scott, D., Silk, J., & White, M. 1995, *Science*, 268, 829
- Scott, P. F., et al. 1996, *ApJ*, 461, L1
- Srednicki, M., White, M., Scott, D., & Bunn, E. F. 1993, *Phys. Rev. Lett.*, 71, 3747
- Stompor, R. 1997, in *Microwave Background Anisotropies*, ed. F. R. Bouchet & T. T. Van (Gif sur Yvette: Editions Frontières), in press
- Stompor, R., Górski, K. M., & Banday, A. J. 1995, *MNRAS*, 277, 1225
- Sugiyama, N. 1995, *ApJS*, 100, 281
- Tanaka, S. T., et al. 1996, *ApJ*, 468, L81 (T96)
- Tanaka, T., & Sasaki, M. 1997, *Prog. Theo. Phys.*, 97, 243

Tucker, G. S., Gush, H. P., Halpern, M., Shinkoda, I., & Towlson, W. 1997, *ApJ*, 475, L73

Turner, M. S. 1997, in *Critical Dialogues in Cosmology*, ed. N. Turok (Singapore: World Scientific),
in press

Yamamoto, K., Sasaki, M., & Tanaka, T. 1995, *ApJ*, 455, 412

Zel'dovich, Ya. B. 1972, *MNRAS*, 160, 1P

Table 1: Numerical Values for the Zero-Lag Window Function Parameters

Channel	$l_{e-0.5}$	l_e	l_m	$l_{e-0.5}$	$\sqrt{I(W_l)}$
MAX 4 3.5 cm^{-1}	80	133	145	224	1.51
MAX 4 6/9 cm^{-1}	70	114	127	196	1.41
MAX 5 3.5 cm^{-1}	83	139	150	232	1.55
MAX 5 6/9 cm^{-1}	80	133	146	224	1.51

Table 2: Numerical Values for Parameters Characterizing the Shape of $(\delta T_{\text{rms}}^2)_l$

W_l :		MAX 4 3.5 cm^{-1}			MAX 4 6/9 cm^{-1}			MAX 5 3.5 cm^{-1}			MAX 5 6/9 cm^{-1}		
#	$(\Omega_0, h, \Omega_B h^2)$	$l_{e^{-.5}}$	l_m	$l_{e^{-.5}}$	$l_{e^{-.5}}$	l_m	$l_{e^{-.5}}$	$l_{e^{-.5}}$	l_m	$l_{e^{-.5}}$	$l_{e^{-.5}}$	l_m	$l_{e^{-.5}}$
(1)	(2)	(3)	(4)	(5)	(6)	(7)	(8)	(9)	(10)	(11)	(12)	(13)	(14)
O1	(0.1, 0.75, 0.0125)	54	130	213	42	110	184	57	135	221	54	130	214
O2	(0.2, 0.65, 0.0175)	66	139	222	54	119	192	69	144	230	66	139	222
O3	(0.2, 0.70, 0.0125)	62	135	219	50	115	189	65	141	228	62	135	220
O4	(0.2, 0.75, 0.0075)	57	131	216	47	111	185	60	136	224	57	131	216
O5	(0.3, 0.60, 0.0175)	70	143	226	58	122	195	73	149	235	70	143	227
O6	(0.3, 0.65, 0.0125)	65	139	224	54	118	193	69	145	233	66	140	224
O7	(0.3, 0.70, 0.0075)	60	135	222	50	114	189	63	140	230	61	135	222
O8	(0.4, 0.60, 0.0175)	71	146	229	59	124	198	75	152	237	71	146	229
O9	(0.4, 0.65, 0.0125)	67	143	227	55	120	195	70	149	235	67	143	227
O10	(0.4, 0.70, 0.0075)	61	139	226	50	115	193	64	145	234	61	139	226
O11	(0.5, 0.55, 0.0175)	75	149	230	62	127	200	78	155	237	75	150	230
O12	(0.5, 0.60, 0.0125)	70	147	229	57	124	198	74	153	236	70	148	229
O13	(0.5, 0.65, 0.0075)	64	145	228	52	120	197	68	151	236	65	145	228
O14	(1.0, 0.50, 0.0125)	81	150	216	66	133	196	85	154	220	81	151	216
$\Lambda 1$	(0.1, 0.90, 0.0125)	85	149	214	74	133	194	88	152	219	85	149	214
$\Lambda 2$	(0.2, 0.80, 0.0075)	85	149	213	73	134	194	88	153	218	85	150	213
$\Lambda 3$	(0.2, 0.75, 0.0125)	85	150	215	74	133	195	88	153	220	86	150	215
$\Lambda 4$	(0.2, 0.70, 0.0175)	86	151	217	75	134	196	89	155	222	86	151	217
$\Lambda 5$	(0.3, 0.70, 0.0075)	85	150	215	71	134	195	88	154	219	85	151	215
$\Lambda 6$	(0.3, 0.65, 0.0125)	85	151	216	73	134	196	88	154	221	85	151	216
$\Lambda 7$	(0.3, 0.60, 0.0175)	86	151	219	74	134	197	89	156	224	86	151	219
$\Lambda 8$	(0.4, 0.65, 0.0075)	84	151	215	70	134	195	87	155	220	84	151	215
$\Lambda 9$	(0.4, 0.60, 0.0125)	85	151	216	72	134	196	88	155	221	85	151	217
$\Lambda 10$	(0.4, 0.55, 0.0175)	86	152	219	74	134	197	89	156	224	86	152	219
$\Lambda 11$	(0.5, 0.60, 0.0125)	84	151	215	71	134	195	87	155	220	84	151	215
Flat	...	41	103	183	36	90	160	42	106	189	41	103	183
W_l	...	80 ^a	133 ^b	224 ^a	70 ^a	114 ^b	196 ^a	83 ^a	139 ^b	232 ^a	80 ^a	133 ^b	224 ^a

^a $l_{e^{-0.5}}$ for the window.

^b l_e for the window.

Table 3: Numerical Values for Rms Temperature Anisotropies^a

Channel	“Sky” ^b	FBP ^c
4ID 3.5 cm ⁻¹	71	86
4ID 6 cm ⁻¹	29	95
4ID 9 cm ⁻¹	55	78
4SH 3.5 cm ⁻¹	89	130
4SH 6 cm ⁻¹	16	0
4SH 9 cm ⁻¹	69	75
5HR 3.5 cm ⁻¹	69	62
5HR 6 cm ⁻¹	44	40
5HR 9 cm ⁻¹	49	56
5PH 3.5 cm ⁻¹	64	78
5PH 6 cm ⁻¹	85	110

^a δT_{rms} in μK .

^bEstimated from the data of Fig. 3, as discussed in §2.

^cConverted to rms from the results of the likelihood analysis for the flat bandpower (FBP) angular spectrum, accounting for beamwidth and calibration uncertainties. Note that the 4ID 9 cm⁻¹ and 4SH 6 cm⁻¹ data sets do not have 2σ HPD detections.

Table 4: Numerical Values for Bandtemperature^a from Likelihood Analyses Assuming a Flat Bandpower Spectrum, for the Individual-Channel Data Sets

Data Set	-1σ	Peak	$+1\sigma$	Ave. Abs. Err. ^b	Ave. Fra. Err. ^c
4ID 3.5 cm ⁻¹	37	57	86	±25	±43%
4ID 6 cm ⁻¹	38	67	110	±37	±55%
4ID 9 cm ⁻¹ ^d	25	55	110	±40	±73%
4SH 3.5 cm ⁻¹	58	86	130	±35	±41%
4SH 6 cm ⁻¹ ^d	0	0	63	±32	...
4SH 9 cm ⁻¹	30	53	91	±31	±58%
5HR 3.5 cm ⁻¹	27	40	58	±15	±38%
5HR 6 cm ⁻¹	20	27	37	±8.7	±33%
5HR 9 cm ⁻¹	25	37	55	±15	±41%
5PH 3.5 cm ⁻¹	32	50	77	±23	±45%
5PH 6 cm ⁻¹	56	74	99	±22	±30%
4 3.5 cm ⁻¹	54	71	93	±19	±28%
4 6 cm ⁻¹	32	55	84	±26	±47%
4 9 cm ⁻¹	35	54	80	±22	±41%
5noMP ^e 3.5 cm ⁻¹	33	44	58	±12	±28%
5noMP ^e 6 cm ⁻¹	41	51	63	±11	±21%

^a δT_l in μK .

^bAverage absolute error in μK .

^cAverage fractional error, as a fraction of the central value.

^d4ID 9 cm⁻¹ and 4SH 6 cm⁻¹ do not have 2σ HPD detections; the appropriate ET 2σ upper limits are 220 μK and 170 μK respectively.

^eData from 5HR and 5PH.

Table 5: Numerical Values for Bandtemperature^a from Likelihood Analyses Assuming a Flat Bandpower Spectrum, for the Combined-Channel Data Sets

Data Set	-1σ	Peak	$+1\sigma$	Ave. Abs. Err. ^b	Ave. Fra. Err. ^c
4ID	38	55	83	± 23	$\pm 41\%$
4SH	58	84	130	± 34	$\pm 40\%$
5HR	22	28	38	± 8.4	$\pm 30\%$
5MP ^d	0	2.1	17	± 8.5	$\pm 410\%$
5PH	56	74	98	± 21	$\pm 28\%$
4	53	69	90	± 19	$\pm 27\%$
5noMP ^e	42	51	63	± 10	$\pm 20\%$
5	37	43	52	± 7.5	$\pm 17\%$
CnoMP ^f	49	58	67	± 9.0	$\pm 16\%$
C ^g	44	51	59	± 7.2	$\pm 14\%$

^a δT_l in μK .

^bAverage absolute error in μK .

^cAverage fractional error, as a fraction of the central value.

^d5MP does not have a 2σ HPD detection. The appropriate ET 2σ upper limit is $42 \mu\text{K}$.

^eData from 5HR and 5PH.

^fC(ombined) data excluding 5MP, i.e., data from 4ID, 4SH, 5HR, and 5PH.

^gC(ombined) data including 5MP.

Table 6: Numerical Values for $Q_{\text{rms-PS}}$ (in μK)^a

Model	$(\Omega_0, h, \Omega_B h^2)$	DMR ^b	4ID	4SH	5HR	5MP	5PH
O1	(0.1, 0.75, 0.0125)	21.0 ^{25.0} _{17.0}	43 ⁶⁴ ₂₉	61 ⁸⁹ ₄₃	23 ³¹ ₁₈	0 ³² _{...}	52 ⁶⁹ ₄₀
O2	(0.2, 0.65, 0.0175)	24.1 ^{28.6} _{19.6}	38 ⁵⁶ ₂₆	54 ⁷⁸ ₃₈	21 ²⁸ ₁₆	0 ²⁸ _{...}	45 ⁶⁰ ₃₅
O3	(0.2, 0.70, 0.0125)	24.1 ^{28.6} _{19.6}	40 ⁵⁹ ₂₇	57 ⁸² ₄₀	22 ²⁹ ₁₇	0 ³⁰ _{...}	48 ⁶³ ₃₇
O4	(0.2, 0.75, 0.0075)	24.1 ^{28.6} _{19.6}	42 ⁶³ ₂₉	60 ⁸⁸ ₄₂	23 ³¹ ₁₈	0 ³¹ _{...}	51 ⁶⁷ ₃₉
O5	(0.3, 0.60, 0.0175)	23.4 ^{27.8} _{19.1}	31 ⁴⁶ ₂₁	44 ⁶³ ₃₁	17 ²³ ₁₃	0 ²³ _{...}	37 ⁴⁹ ₂₈
O6	(0.3, 0.65, 0.0125)	23.4 ^{27.8} _{19.1}	33 ⁴⁹ ₂₃	47 ⁶⁸ ₃₃	18 ²⁴ ₁₄	0 ²⁴ _{...}	39 ⁵² ₃₀
O7	(0.3, 0.70, 0.0075)	23.4 ^{27.8} _{19.1}	35 ⁵² ₂₄	50 ⁷³ ₃₅	19 ²⁶ ₁₅	0 ²⁶ _{...}	42 ⁵⁶ ₃₃
O8	(0.4, 0.60, 0.0175)	21.2 ^{24.9} _{17.4}	25 ³⁷ ₁₇	36 ⁵² ₂₅	14 ¹⁹ ₁₁	0 ¹⁹ _{...}	30 ⁴⁰ ₂₃
O9	(0.4, 0.65, 0.0125)	21.2 ^{24.9} _{17.4}	27 ⁴⁰ ₁₈	38 ⁵⁶ ₂₇	15 ²⁰ ₁₁	0 ²⁰ _{...}	32 ⁴³ ₂₅
O10	(0.4, 0.70, 0.0075)	21.2 ^{24.9} _{17.4}	29 ⁴³ ₂₀	41 ⁶⁰ ₂₉	16 ²² ₁₂	0 ²¹ _{...}	35 ⁴⁶ ₂₇
O11	(0.5, 0.55, 0.0175)	18.5 ^{21.7} _{15.3}	20 ²⁹ ₁₃	28 ⁴¹ ₂₀	11 ¹⁵ _{8.5}	0 ¹⁴ _{...}	24 ³¹ ₁₈
O12	(0.5, 0.60, 0.0125)	18.5 ^{21.7} _{15.3}	21 ³² ₁₅	30 ⁴⁴ ₂₁	12 ¹⁶ _{9.1}	0 ¹⁶ _{...}	26 ³⁴ ₂₀
O13	(0.5, 0.65, 0.0075)	18.5 ^{21.7} _{15.3}	23 ³⁴ ₁₆	33 ⁴⁸ ₂₃	13 ¹⁷ _{9.8}	0 ¹⁷ _{...}	28 ³⁷ ₂₂
O14	(1.0, 0.50, 0.0125)	17.8 ^{20.8} _{14.7}	18 ²⁷ ₁₂	27 ⁴⁰ ₁₉	10 ¹⁴ _{7.9}	0 ¹⁴ _{...}	23 ³¹ ₁₈
Λ 1	(0.1, 0.90, 0.0125)	25.5 ^{29.7} _{21.2}	20 ³⁰ ₁₄	30 ⁴⁴ ₂₀	12 ¹⁶ _{8.8}	0 ¹⁵ _{...}	26 ³⁴ ₂₀
Λ 2	(0.2, 0.80, 0.0075)	23.3 ^{27.1} _{19.4}	20 ³⁰ ₁₄	30 ⁴⁴ ₂₁	12 ¹⁶ _{8.8}	0 ¹⁵ _{...}	26 ³⁴ ₂₀
Λ 3	(0.2, 0.75, 0.0125)	23.1 ^{27.0} _{19.2}	19 ²⁸ ₁₃	27 ⁴¹ ₁₉	11 ¹⁴ _{8.1}	0 ¹⁴ _{...}	24 ³¹ ₁₈
Λ 4	(0.2, 0.70, 0.0175)	23.0 ^{26.8} _{19.1}	17 ²⁶ ₁₂	25 ³⁸ ₁₇	10 ¹³ _{7.6}	0 ¹³ _{...}	22 ²⁹ ₁₇
Λ 5	(0.3, 0.70, 0.0075)	21.0 ^{24.5} _{17.5}	19 ²⁸ ₁₃	28 ⁴² ₁₉	11 ¹⁵ _{8.2}	0 ¹⁴ _{...}	24 ³² ₁₈
Λ 6	(0.3, 0.65, 0.0125)	21.0 ^{24.5} _{17.4}	17 ²⁶ ₁₂	26 ³⁸ ₁₈	10 ¹³ _{7.6}	0 ¹³ _{...}	22 ²⁹ ₁₇
Λ 7	(0.3, 0.60, 0.0175)	20.9 ^{24.4} _{17.4}	16 ²⁴ ₁₁	24 ³⁵ ₁₆	9.3 ¹² _{7.1}	0 ¹² _{...}	20 ²⁷ ₁₆
Λ 8	(0.4, 0.65, 0.0075)	19.4 ^{22.7} _{16.1}	18 ²⁸ ₁₃	27 ⁴¹ ₁₉	11 ¹⁴ _{8.0}	0 ¹⁴ _{...}	23 ³¹ ₁₈
Λ 9	(0.4, 0.60, 0.0125)	19.4 ^{22.7} _{16.1}	17 ²⁵ ₁₂	25 ³⁷ ₁₇	9.7 ¹³ _{7.4}	0 ¹³ _{...}	21 ²⁸ ₁₆
Λ 10	(0.4, 0.55, 0.0175)	19.4 ^{22.7} _{16.1}	15 ²³ ₁₁	23 ³⁴ ₁₆	9.0 ¹² _{6.8}	0 ¹² _{...}	19 ²⁶ ₁₅
Λ 11	(0.5, 0.60, 0.0125)	18.5 ^{21.6} _{15.3}	17 ²⁶ ₁₂	25 ³⁸ ₁₇	9.8 ¹³ _{7.5}	0 ¹³ _{...}	22 ²⁹ ₁₇
Flat	...	18.6 ^{21.8} _{15.4}	36 ⁵³ ₂₄	54 ⁸¹ ₃₇	18 ²⁵ ₁₄	1.3 ²⁷ _{...}	47 ⁶³ ₃₆

^aFor each model, the first of the three entries in each of the last six columns is where the probability density distribution function peaks. Ellipses as the lower entry in a vertical pair denotes a non-detection; the upper entry then is the 2σ (97.7% ET) upper limit. For detections, the vertical pair of numbers are the $\pm 1\sigma$ (68.3% HPD) limits, except for DMR where they are $\pm 2\sigma$ (95.5% HPD).

^bDMR values are from Górski et al. (1996,1998) and Stompor (1997).

Table 7: Numerical Values for $Q_{\text{rms-PS}}$ (in μK)^a

Model	$(\Omega_0, h, \Omega_B h^2)$	DMR	4	5noMP ^b	5	CnoMP ^c	C ^d
O1	(0.1, 0.75, 0.0125)	21.0 ^{25.0} _{17.0}	52 ⁶⁷ ₄₀	38 ⁴⁶ ₃₁	32 ³⁸ ₂₇	43 ⁵⁰ ₃₇	38 ⁴⁴ ₃₃
O2	(0.2, 0.65, 0.0175)	24.1 ^{28.6} _{19.6}	46 ⁵⁹ ₃₆	33 ⁴⁰ ₂₈	28 ³⁴ ₂₄	38 ⁴⁴ ₃₂	33 ³⁸ ₂₉
O3	(0.2, 0.70, 0.0125)	24.1 ^{28.6} _{19.6}	48 ⁶² ₃₇	35 ⁴² ₂₉	30 ³⁵ ₂₅	40 ⁴⁶ ₃₄	35 ⁴⁰ ₃₁
O4	(0.2, 0.75, 0.0075)	24.1 ^{28.6} _{19.6}	51 ⁶⁶ ₄₀	37 ⁴⁵ ₃₁	32 ³⁸ ₂₇	42 ⁴⁹ ₃₆	37 ⁴³ ₃₂
O5	(0.3, 0.60, 0.0175)	23.4 ^{27.8} _{19.1}	37 ⁴⁸ ₂₉	27 ³³ ₂₃	23 ²⁸ ₂₀	31 ³⁶ ₂₆	27 ³¹ ₂₄
O6	(0.3, 0.65, 0.0125)	23.4 ^{27.8} _{19.1}	40 ⁵¹ ₃₁	29 ³⁵ ₂₄	25 ²⁹ ₂₁	33 ³⁸ ₂₈	29 ³³ ₂₅
O7	(0.3, 0.70, 0.0075)	23.4 ^{27.8} _{19.1}	42 ⁵⁵ ₃₃	31 ³⁸ ₂₆	27 ³¹ ₂₃	35 ⁴¹ ₃₀	31 ³⁶ ₂₇
O8	(0.4, 0.60, 0.0175)	21.2 ^{24.9} _{17.4}	30 ³⁹ ₂₄	22 ²⁷ ₁₈	19 ²² ₁₆	25 ²⁹ ₂₂	22 ²⁶ ₁₉
O9	(0.4, 0.65, 0.0125)	21.2 ^{24.9} _{17.4}	32 ⁴² ₂₅	24 ²⁹ ₂₀	20 ²⁴ ₁₇	27 ³¹ ₂₃	24 ²⁷ ₂₁
O10	(0.4, 0.70, 0.0075)	21.2 ^{24.9} _{17.4}	35 ⁴⁶ ₂₇	26 ³¹ ₂₁	22 ²⁶ ₁₉	29 ³⁴ ₂₅	26 ³⁰ ₂₂
O11	(0.5, 0.55, 0.0175)	18.5 ^{21.7} _{15.3}	24 ³¹ ₁₈	17 ²¹ ₁₅	15 ¹⁸ ₁₃	20 ²³ ₁₇	17 ²⁰ ₁₅
O12	(0.5, 0.60, 0.0125)	18.5 ^{21.7} _{15.3}	26 ³³ ₂₀	19 ²³ ₁₆	16 ¹⁹ ₁₄	21 ²⁵ ₁₈	19 ²² ₁₆
O13	(0.5, 0.65, 0.0075)	18.5 ^{21.7} _{15.3}	28 ³⁶ ₂₂	20 ²⁵ ₁₇	18 ²¹ ₁₅	23 ²⁷ ₂₀	20 ²⁴ ₁₈
O14	(1.0, 0.50, 0.0125)	17.8 ^{20.8} _{14.7}	22 ²⁹ ₁₇	17 ²¹ ₁₄	14 ¹⁷ ₁₂	19 ²² ₁₆	17 ¹⁹ ₁₄
Λ 1	(0.1, 0.90, 0.0125)	25.5 ^{29.7} _{21.2}	25 ³² ₁₉	19 ²³ ₁₆	16 ¹⁹ ₁₄	21 ²⁴ ₁₈	18 ²¹ ₁₆
Λ 2	(0.2, 0.80, 0.0075)	23.3 ^{27.1} _{19.4}	25 ³² ₁₉	19 ²³ ₁₆	16 ¹⁹ ₁₄	21 ²⁴ ₁₈	18 ²¹ ₁₆
Λ 3	(0.2, 0.75, 0.0125)	23.1 ^{27.0} _{19.2}	23 ³⁰ ₁₈	17 ²¹ ₁₄	15 ¹⁷ ₁₂	19 ²² ₁₇	17 ²⁰ ₁₅
Λ 4	(0.2, 0.70, 0.0175)	23.0 ^{26.8} _{19.1}	21 ²⁸ ₁₆	16 ¹⁹ ₁₃	14 ¹⁶ ₁₂	18 ²¹ ₁₅	16 ¹⁸ ₁₄
Λ 5	(0.3, 0.70, 0.0075)	21.0 ^{24.5} _{17.5}	23 ³⁰ ₁₈	18 ²¹ ₁₅	15 ¹⁸ ₁₃	20 ²³ ₁₇	17 ²⁰ ₁₅
Λ 6	(0.3, 0.65, 0.0125)	21.0 ^{24.5} _{17.4}	21 ²⁸ ₁₆	16 ²⁰ ₁₃	14 ¹⁶ ₁₂	18 ²¹ ₁₅	16 ¹⁸ ₁₄
Λ 7	(0.3, 0.60, 0.0175)	20.9 ^{24.4} _{17.4}	20 ²⁶ ₁₅	15 ¹⁸ ₁₂	13 ¹⁵ ₁₁	16 ¹⁹ ₁₄	15 ¹⁷ ₁₃
Λ 8	(0.4, 0.65, 0.0075)	19.4 ^{22.7} _{16.1}	23 ³⁰ ₁₇	17 ²¹ ₁₄	15 ¹⁷ ₁₂	19 ²² ₁₆	17 ¹⁹ ₁₅
Λ 9	(0.4, 0.60, 0.0125)	19.4 ^{22.7} _{16.1}	21 ²⁷ ₁₆	16 ¹⁹ ₁₃	13 ¹⁶ ₁₁	17 ²⁰ ₁₅	15 ¹⁸ ₁₃
Λ 10	(0.4, 0.55, 0.0175)	19.4 ^{22.7} _{16.1}	19 ²⁵ ₁₅	14 ¹⁷ ₁₂	12 ¹⁴ ₁₀	16 ¹⁹ ₁₄	14 ¹⁶ ₁₂
Λ 11	(0.5, 0.60, 0.0125)	18.5 ^{21.6} _{15.3}	21 ²⁸ ₁₆	16 ¹⁹ ₁₃	14 ¹⁶ ₁₂	18 ²¹ ₁₅	16 ¹⁸ ₁₄
Flat	...	18.6 ^{21.8} _{15.4}	44 ⁵⁸ ₃₄	33 ⁴¹ ₂₇	28 ³³ ₂₄	37 ⁴³ ₃₂	33 ³⁸ ₂₈

^aConventions are the same as for Table 6.

^bData from 5HR and 5PH.

^cC(ombined) data excluding 5MP.

^dC(ombined) data including 5MP.

Table 8: Renormalized Maximum Values of the Probability Density Distribution Functions^a

Model	4ID	4SH	5HR	5MP	5PH	4	5noMP	5	CnoMP	C
O1	0.92	0.90	1.0	1.0	0.66	0.95	0.72	0.89	0.75	0.88
O2	0.87	0.98	0.70	1.0	0.66	0.99	0.61	0.76	0.67	0.78
O3	0.88	0.96	0.79	1.0	0.66	0.98	0.65	0.81	0.70	0.82
O4	0.90	0.93	0.90	1.0	0.66	0.97	0.69	0.85	0.73	0.85
O5	0.85	1.0	0.61	1.0	0.69	1.0	0.61	0.73	0.67	0.76
O6	0.87	0.98	0.70	1.0	0.70	0.99	0.66	0.79	0.72	0.82
O7	0.88	0.96	0.80	1.0	0.70	0.98	0.70	0.85	0.77	0.87
O8	0.85	0.98	0.60	1.0	0.76	0.99	0.67	0.77	0.75	0.81
O9	0.87	0.96	0.69	1.0	0.78	0.98	0.74	0.85	0.82	0.88
O10	0.88	0.95	0.79	1.0	0.79	0.97	0.79	0.92	0.87	0.95
O11	0.86	0.96	0.58	1.0	0.82	0.97	0.72	0.78	0.80	0.83
O12	0.88	0.94	0.66	1.0	0.85	0.96	0.79	0.87	0.88	0.92
O13	0.89	0.93	0.75	1.0	0.86	0.96	0.86	0.96	0.95	1.0
O14	0.99	0.71	0.83	1.0	1.0	0.79	1.0	1.0	1.0	1.0
Λ 1	0.99	0.70	0.74	1.0	0.97	0.77	0.91	0.86	0.90	0.86
Λ 2	1.0	0.69	0.78	1.0	0.96	0.77	0.92	0.90	0.91	0.89
Λ 3	0.99	0.71	0.74	1.0	0.98	0.78	0.92	0.88	0.92	0.89
Λ 4	0.96	0.73	0.67	1.0	0.99	0.79	0.90	0.86	0.92	0.87
Λ 5	0.99	0.71	0.77	1.0	0.97	0.79	0.93	0.91	0.92	0.91
Λ 6	0.98	0.72	0.72	1.0	0.99	0.79	0.92	0.90	0.93	0.90
Λ 7	0.96	0.75	0.65	1.0	1.00	0.81	0.90	0.86	0.92	0.88
Λ 8	0.99	0.71	0.78	1.0	0.97	0.79	0.94	0.93	0.94	0.93
Λ 9	0.98	0.73	0.73	1.0	0.99	0.79	0.94	0.91	0.94	0.92
Λ 10	0.96	0.76	0.65	1.0	1.0	0.81	0.91	0.87	0.93	0.89
Λ 11	0.99	0.71	0.78	1.0	0.99	0.78	0.96	0.94	0.96	0.94
Flat	1.1	0.61	2.6	1.0	0.58	0.71	0.78	0.78	0.68	0.66
...	$1 \cdot 10^6$	$5 \cdot 10^{12}$	$3 \cdot 10^{19}$	$1 \cdot 10^0$	$7 \cdot 10^{34}$	$4 \cdot 10^{18}$	$2 \cdot 10^{53}$	$6 \cdot 10^{51}$	$4 \cdot 10^{71}$	$6 \cdot 10^{69}$

^aRenormalized such that it is unity for the “realistic” model with the highest maximum value of the probability density distribution function for the data set. The last line of the table gives this highest maximum likelihood value when the normalization is set such that $L(Q_{\text{rms-PS}} = 0 \mu\text{K}) = 1$.

Table 9: Renormalized Marginal Values of the Probability Density Distribution Functions^a

Model	4ID	4SH	5HR	5MP	5PH	4	5noMP	5	CnoMP	C
O1	1.0	0.99	1.0	1.0	1.0	1.0	1.0	1.0	1.0	1.0
O2	0.83	0.93	0.63	0.88	0.86	0.91	0.74	0.75	0.77	0.78
O3	0.89	0.96	0.74	0.93	0.92	0.95	0.84	0.84	0.86	0.86
O4	0.96	1.0	0.89	0.98	0.97	0.99	0.94	0.94	0.95	0.95
O5	0.67	0.77	0.45	0.71	0.73	0.75	0.60	0.58	0.64	0.62
O6	0.72	0.81	0.55	0.76	0.80	0.79	0.70	0.67	0.73	0.71
O7	0.79	0.86	0.67	0.82	0.86	0.84	0.80	0.78	0.83	0.81
O8	0.55	0.62	0.37	0.58	0.65	0.60	0.55	0.50	0.58	0.53
O9	0.60	0.66	0.45	0.62	0.73	0.64	0.64	0.59	0.68	0.63
O10	0.65	0.71	0.54	0.67	0.80	0.69	0.75	0.70	0.79	0.73
O11	0.43	0.49	0.28	0.45	0.56	0.47	0.46	0.40	0.49	0.43
O12	0.48	0.52	0.34	0.49	0.63	0.50	0.56	0.49	0.58	0.52
O13	0.52	0.56	0.42	0.53	0.70	0.54	0.65	0.58	0.68	0.61
O14	0.47	0.36	0.38	0.42	0.67	0.37	0.63	0.50	0.59	0.50
Λ1	0.51	0.39	0.38	0.46	0.73	0.39	0.64	0.48	0.59	0.48
Λ2	0.52	0.39	0.40	0.47	0.72	0.40	0.64	0.49	0.59	0.49
Λ3	0.47	0.37	0.35	0.43	0.68	0.37	0.59	0.45	0.55	0.45
Λ4	0.43	0.35	0.29	0.40	0.63	0.35	0.54	0.40	0.51	0.41
Λ5	0.48	0.38	0.36	0.44	0.68	0.38	0.61	0.47	0.57	0.47
Λ6	0.44	0.35	0.31	0.40	0.64	0.35	0.56	0.43	0.53	0.43
Λ7	0.40	0.33	0.26	0.37	0.59	0.33	0.50	0.37	0.48	0.38
Λ8	0.47	0.37	0.36	0.43	0.66	0.37	0.60	0.47	0.56	0.47
Λ9	0.43	0.34	0.31	0.39	0.62	0.34	0.54	0.42	0.52	0.42
Λ10	0.38	0.32	0.26	0.36	0.57	0.32	0.49	0.37	0.47	0.38
Λ11	0.44	0.34	0.33	0.40	0.63	0.34	0.57	0.44	0.53	0.44
Flat	1.0	0.62	2.1	0.84	0.82	0.66	0.98	0.78	0.81	0.66
...	$5 \cdot 10^7$	$3 \cdot 10^{14}$	$5 \cdot 10^{20}$	$2 \cdot 10^1$	$2 \cdot 10^{36}$	$1 \cdot 10^{20}$	$2 \cdot 10^{54}$	$7 \cdot 10^{52}$	$5 \cdot 10^{72}$	$7 \cdot 10^{70}$

^aRenormalized such that it is unity for the “realistic” model with the highest marginal probability density distribution function value for the data set. The last line of the table gives the marginal value for the model with highest marginal probability density distribution function value when the likelihoods are normalized such that $L(Q_{\text{rms-PS}} = 0 \mu\text{K}) = 1$.

FIGURE CAPTIONS

Fig. 1.— CMB anisotropy multipole moments $l(l+1)C_l/(2\pi) \times 10^{10}$ (broken lines, scale on left axis) as a function of multipole l , to $l = 600$, for selected models O1, O11, O14, $\Lambda 2$, $\Lambda 10$, and Flat, normalized to the DMR maps (Górski et al. 1996,1998; Stompor 1997). See Table 6 for model-parameter values. Also shown are the four MAX individual-channel, zero-lag, nominal beamwidth window functions W_l (solid lines, scale on right axis): MAX 4 6/9 cm^{-1} ; MAX 4 3.5 cm^{-1} ; MAX 5 6/9 cm^{-1} ; and MAX 5 3.5 cm^{-1} with the W_l peak moving from left to right (the MAX 4 3.5 cm^{-1} and MAX 5 6/9 cm^{-1} window functions overlap).

Fig. 2.— $(\delta T_{\text{rms}}^2)_l [= T_0^2(2l+1)C_l W_l/(4\pi)]$, where T_0 is the CMB temperature now] as a function of l , to $l = 400$, for (upper panel) the MAX 4 6/9 cm^{-1} W_l , and for (lower panel) the MAX 5 3.5 cm^{-1} W_l , for the selected models shown in Fig. 1, normalized to the DMR data. See Tables 2, 6, and 7 for numerical values. Note that the peak sensitivity of an individual-channel window function corresponds to a different angular scale in each of the models.

Fig. 3.— Individual-channel MAX data (thermodynamic temperature).

Fig. 4.— Likelihood functions, as a function of $Q_{\text{rms-PS}}$ for the 6 selected models (O1, O11, O14, $\Lambda 2$, $\Lambda 10$, and Flat) of Fig. 1 (line styles are identical to those used in Figs. 1 and 2), for the combined-channel MAX data sets. See Table 2 for model-parameter values, and Tables 6 – 9 for numerical values derived from the corresponding probability density distribution functions.

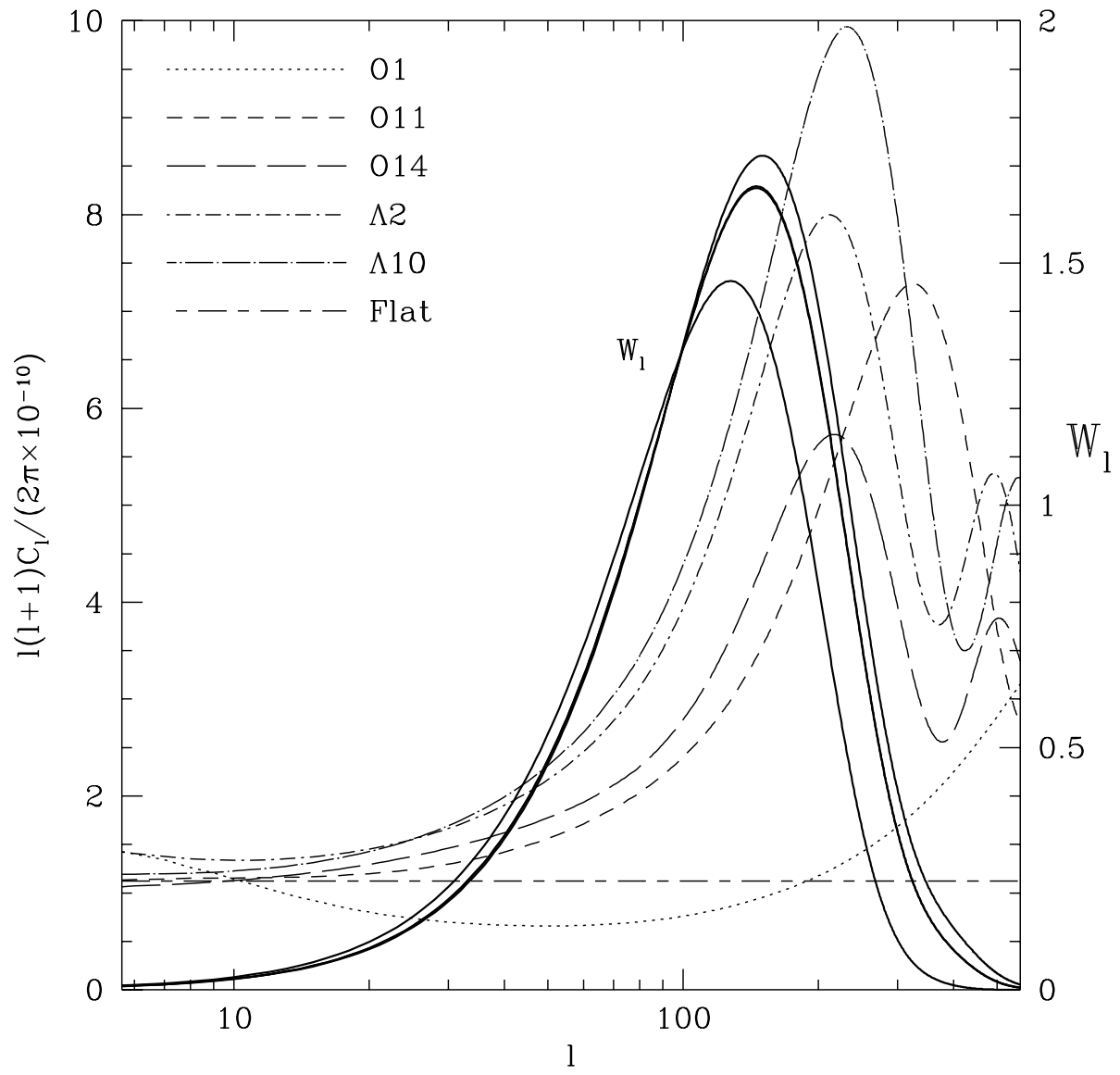


Figure 1

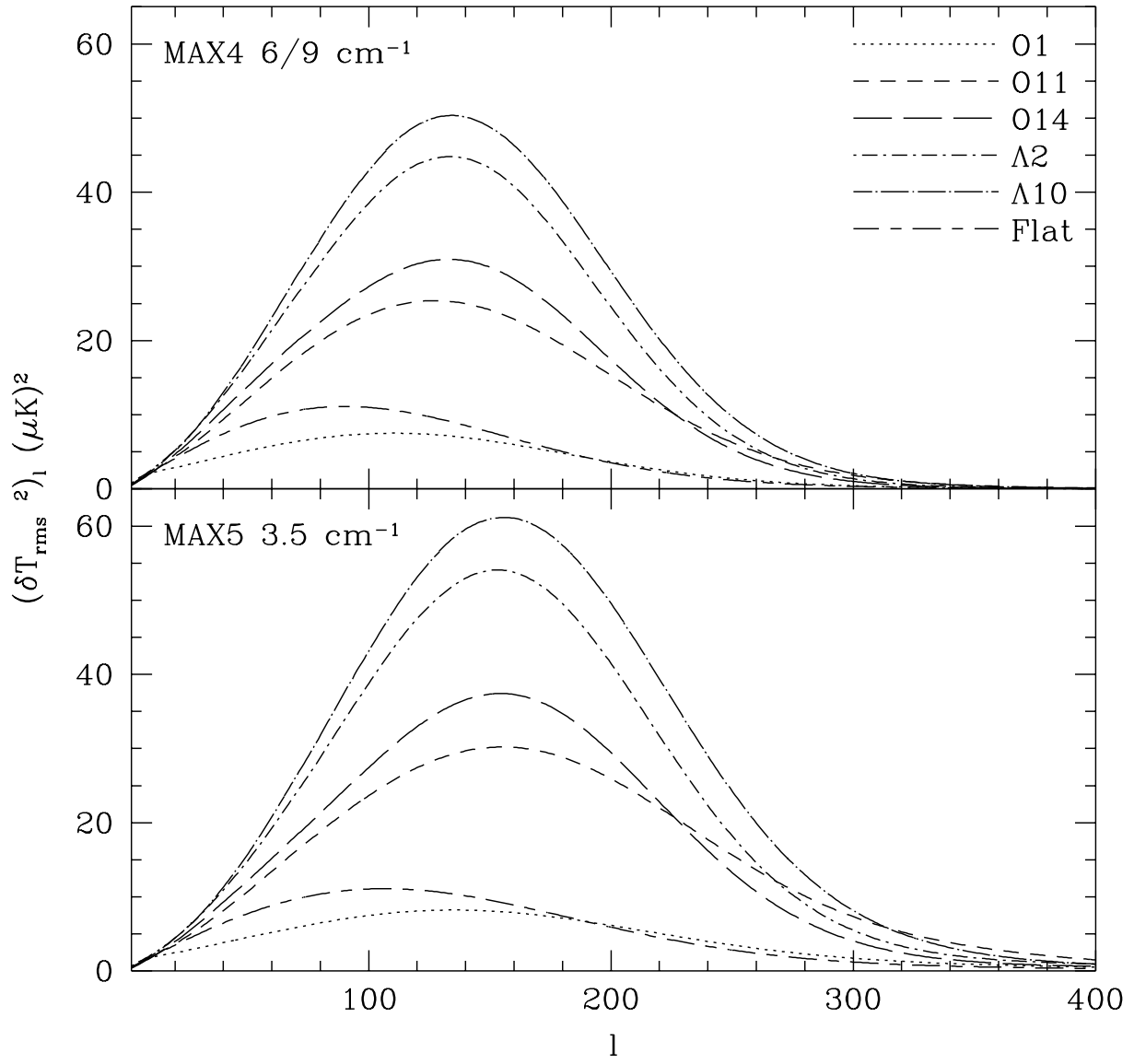


Figure 2

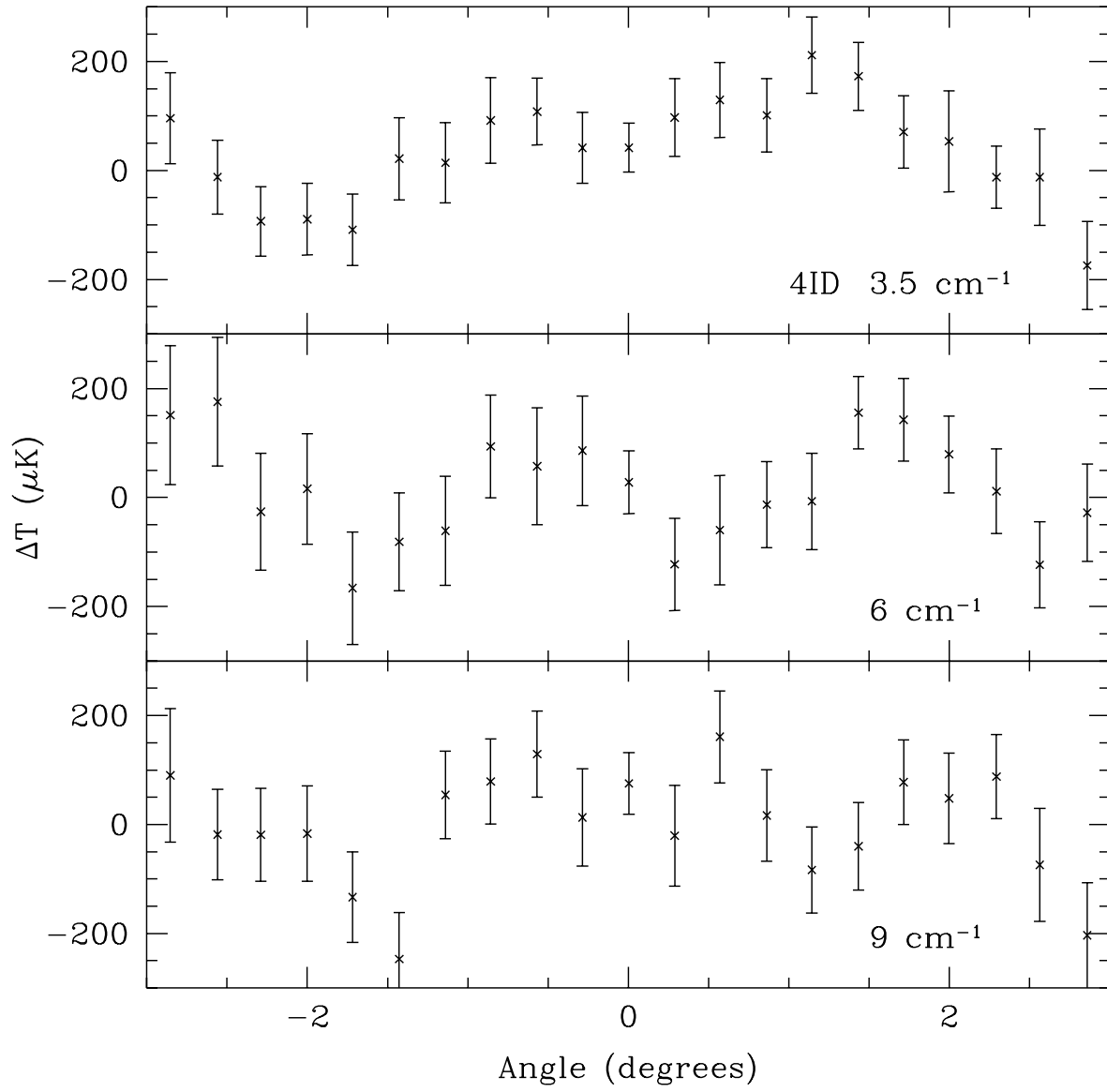


Figure 3a

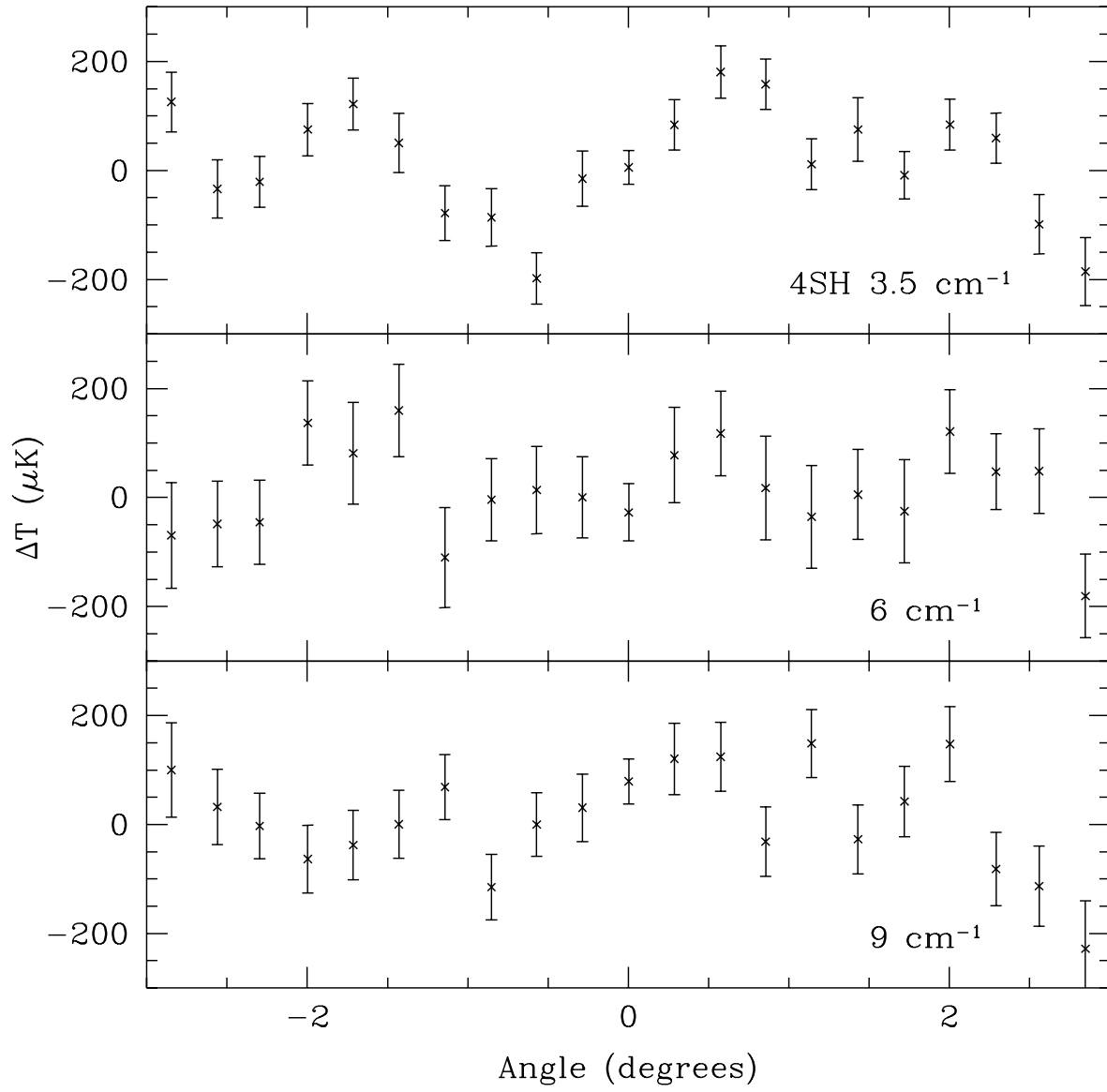


Figure 3b

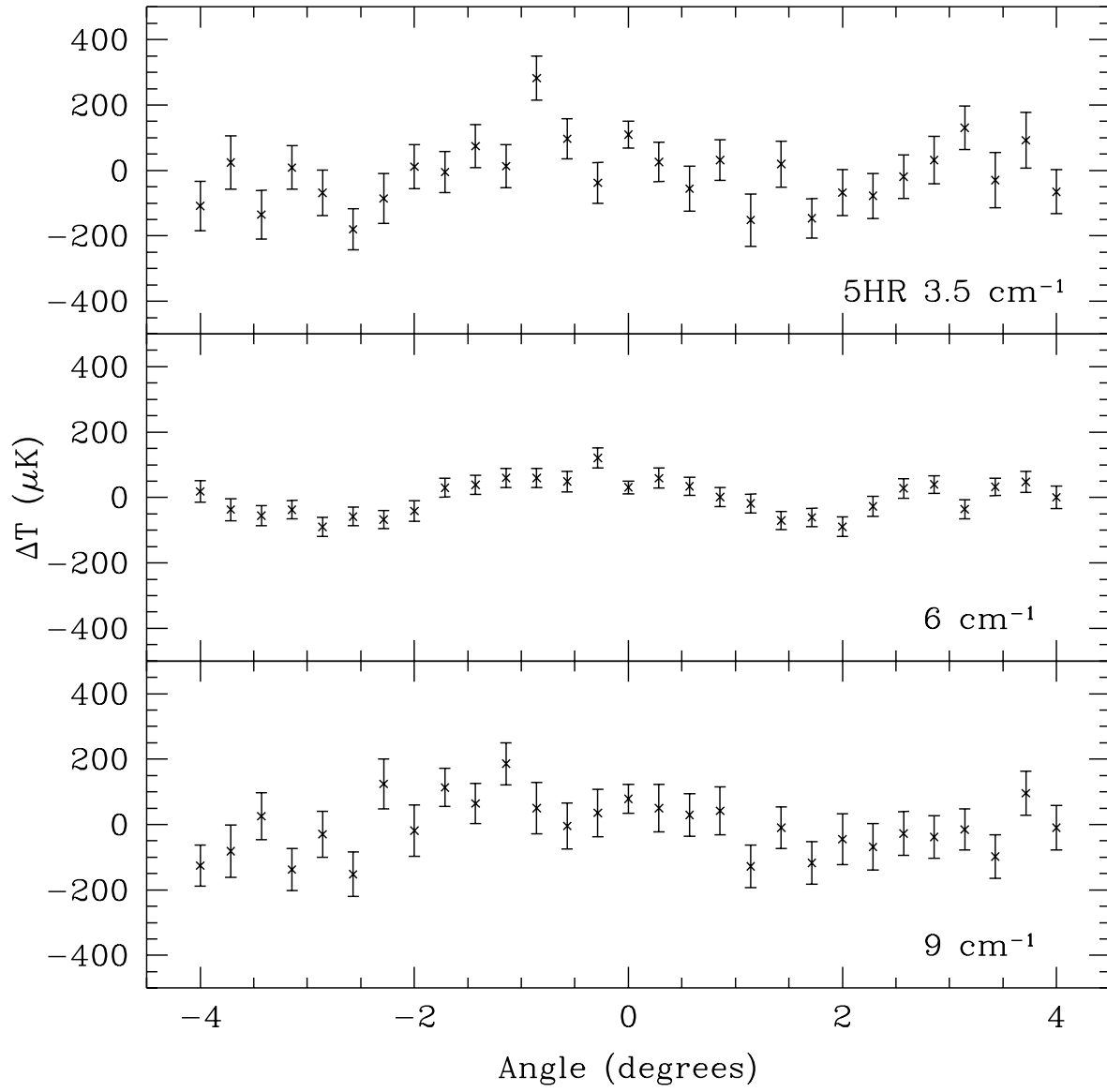


Figure 3c

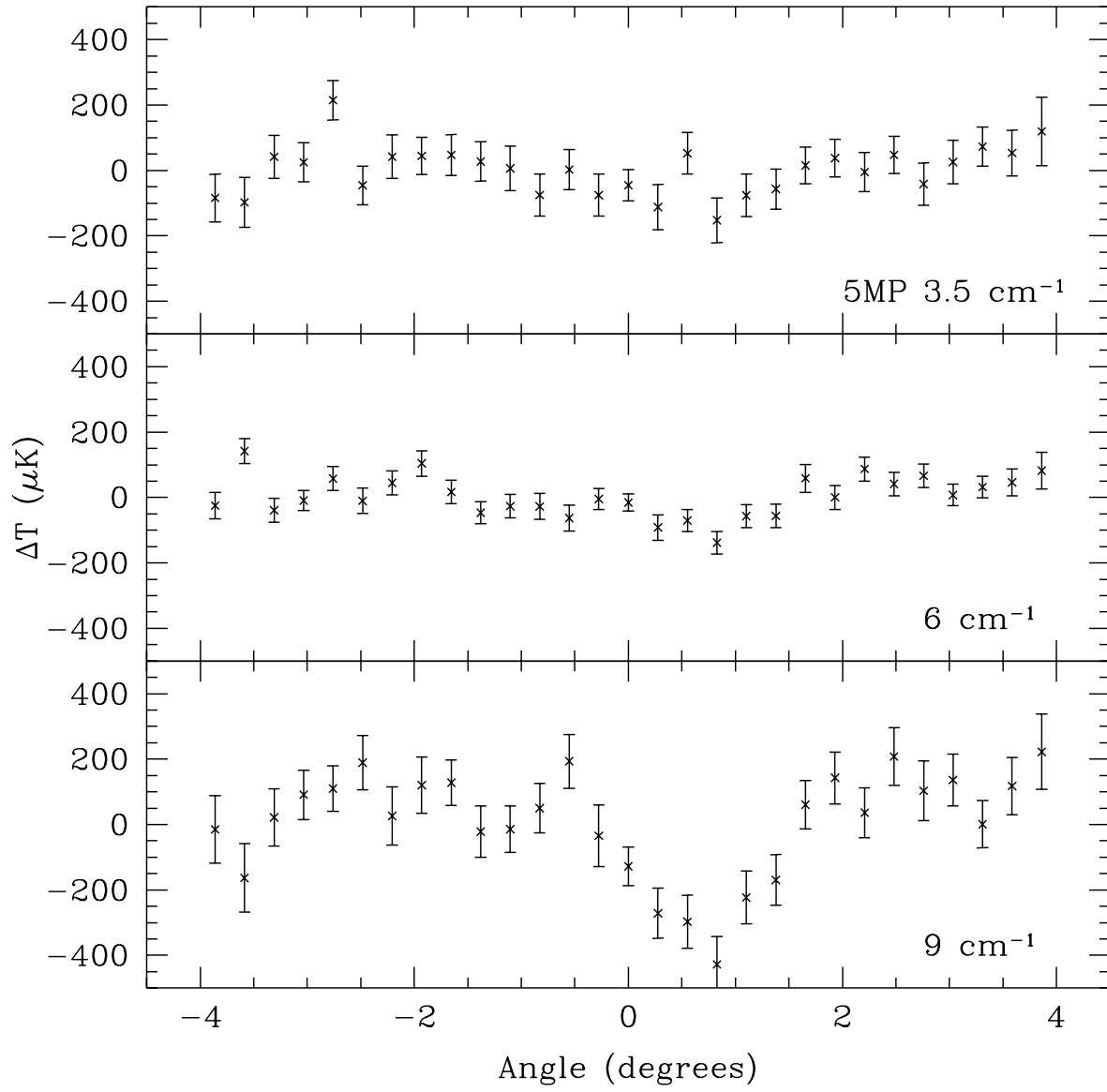


Figure 3d

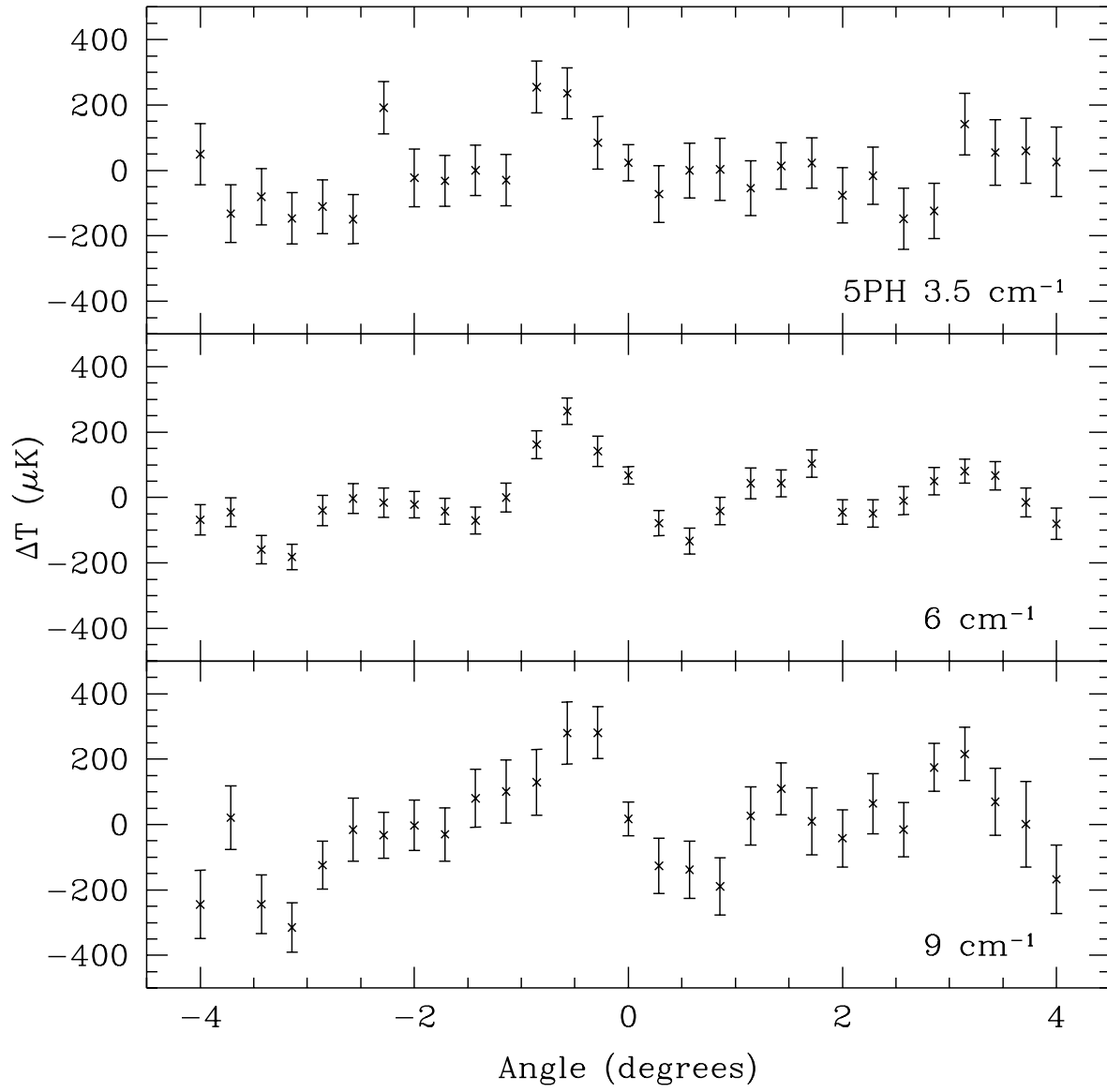


Figure 3e

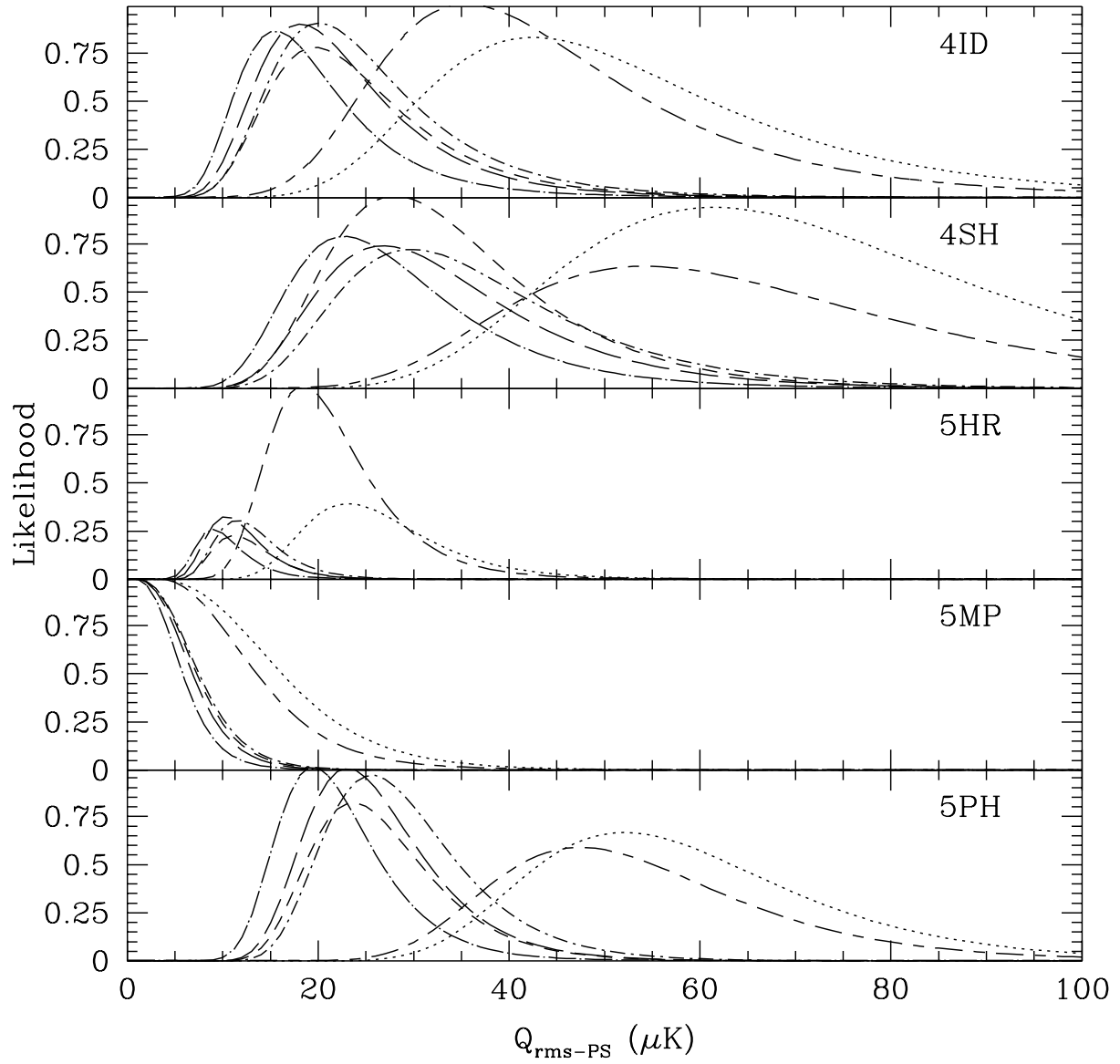


Figure 4a

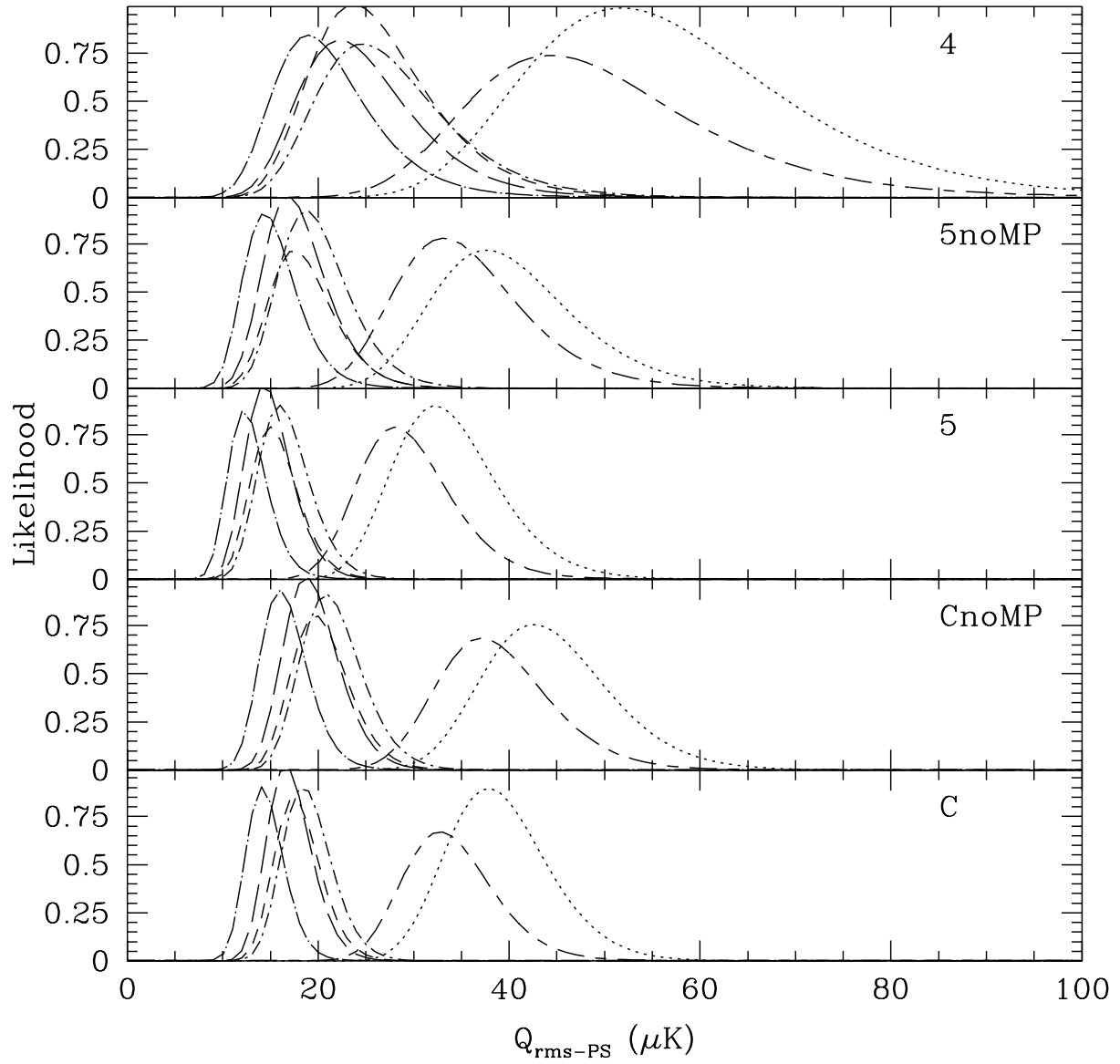


Figure 4b